Tampereen yliopisto

Jarkko Kilpeläinen

HYPERSPECTRAL DIGITAL HOLOGRAPHY FOR BIO-TISSUE SEGMENTATION

Department of Signal Processing, Tampere University
Bachelor's Thesis
November 2019

ABSTRACT

Jarkko Kilpeläinen: Hyperspectral digital holography for bio-tissue segmentation
Bachelor's thesis
Tampere University
BSc (Tech), Electrical Engineering
November 2019

Hyperspectral digital holography is a relatively new imaging method. This work discusses and demonstrates its advantages compared to traditional imaging methods. The main problem with current imaging systems is that they do not capture transparent objects or their shapes very well. This is especially important in cells and tissues, which consist mostly of water and are thus transparent. Holography has the advantage of utilizing the full complex amplitude, instead of just its intensity. It can be utilized in different detection and segmentation problems, but here the focus is in biotechnology and tissue segmentation.

The hyperspectral imaging process in this work consists of capturing diffracted images of the sample at different wavelengths, backpropagating the diffracted images to correct focus and then segmenting the acquired image stack. A lensless capturing setup is used, which has the advantage of having no chromatic aberration. The imaging process in an adaptation of the Fourier transform spectrometer, which requires only one scan to get the full hyperspectral holographic information. The phase delay for the spectrometer is created by adjusting the optical distance of one of the wavefronts in the system. This is done by a mirror controlled by a piezotransducer. To be able to capture hyperspectral information, a supercontinuum laser source is used. The backpropagation is performed with the angular spectrum method, which is computationally efficient. Segmentation is done using k-means clustering in MATLAB.

The results show that hyperspectral digital holography is better for capturing transparent objects due to the phase information and wide wavelength spectra. Some of the possible error sources and complications in the process are also discussed.

Chapter 1 looks at some of the most recent studies regarding the subject. Chapter 2 describes the theory of wave optics and Fourier transforms necessary for this work. Chapter 3 illustrates the practical process for capturing, reconstructing and segmenting the images. In chapter 4 the resulting segmented images are discussed and chapter 5 concludes the work.

The originality of this thesis has been checked using the Turnitin OriginalityCheck service.

TIIVISTELMÄ

Jarkko Kilpeläinen: Kudosten segmentointi hyperspektraalin digitaalisen holografian avulla
Kandidaatintyö
Tampereen yliopisto
Tieto- ja sähkötekniikan TkK-tutkinto-ohjelma, Sähkötekniikka
Marraskuu 2019

Hyperspektraali digitaalinen holografia on verrattain uusi kuvantamismenetelmä. Tässä työssä tutkitaan ja esitellään sen etuja perinteisiin kuvantamismenetelmiin verrattuna. Suurin ongelma nykyisissä kuvausjärjestelmissä on niiden huono kyky erottaa läpinäkyviä kohteita tai niiden muotoja. Tämä on erityisen merkittävää soluissa ja kudoksissa, jotka koostuvat suurimmaksi osaksi vedestä ja ovat siten hyvin läpinäkyviä. Holografian etu on että se käyttää koko kompleksiamplitudia pelkän intensiteetin sijaan. Sitä voidaan hyödyntää erilaisissa tunnistus- tai segmentointitehtävissä, mutta tässä työssä keskitytään bioteknologiaan ja kudosten segmentointiin.

Tämän työn hyperspektraali kuvantamisprosessi koostuu diffraktoituneiden kuvien tallentamisesta eri aallonpituuksilla, näiden kuvien tarkentamisesta takaisin oikeaan tasoon ja lopulta koko kuvapinon segmentoinnista. Työssä käytetään linssitöntä kuvausjärjestelmää, jolloin vältetään väriaberraatio-ongelmat. Kuvausprosessi on sovellutus Fourier-muunnosspektrometristä, jolloin koko hyperspektraali holografinen informaatio voidaan tallentaa yhdellä skannauksella. Spektrometrin vaihesiirto saadaan aikaan säätämällä toisen aaltorintaman kulkemaa optista matkaa. Tätä varten käytetään piezo-ohjattua peiliä. Jotta hyperspektraalia informaatiota voidaan tallentaa, käytetään supercontinuum –laserlähdettä. Diffraktoituneiden kuvien heijastus takaisin oikeaan tasoon suoritetaan kulmaspektrimetodia käyttäen, joka on laskennallisesti tehokas. Segmentointi tehdään MATLAB:in kmeans –klusterointia käyttäen.

Tulokset osoittavat että hyperspektraali digitaalinen holografia on parempi tallentamaan läpinäkyviä kohteita vaiheinformaation ja laajemman aallonpituusspektrin vuoksi. Virhelähteitä ja tallentamisprosessiin liittyviä haasteita käsitellään myös lyhyesti.

Kappaleessa 1 käsitellään uusimpia tutkimuksia aiheeseen liittyen. Kappaleessa 2 kerrotaan työssä tarvittavan aalto-optiikan ja Fourier-muunnosten teoria. Kappaleessa 3 käydään läpi käytännön prosessi kuvien tallentamiseen, rekonstruointiin ja segmentointiin. Kappaleessa 4 esitellään saadut segmentointikuvat sekä tutkitaan tuloksia ja kappale 5 saattaa työn päätökseen.

CONTENTS

ABBREVIATIONS

HIS	Hyperspectral imaging system
HSDH	Hyperspectral digital holography
CCD	Charge-coupled device, Imaging technology used in digital cam eras
FFT	Fast Fourier transform, a computationally efficient method for calculating the discrete Fourier transform
Supercontinuum	Light that is spatially coherent and has broad spectrum

.

1. INTRODUCTION

Light is a complex wavefront with amplitude and phase. Traditional imaging systems, such as digital cameras, only record the intensity of light reflected or transmitted by an object. In this case the depth and thickness information of the object is irrecoverably lost. A holographic recording contains complete spatial information of an object, including intensity and phase. Holography was first invented by Gabor in 1948 [1]. The holographic recording can be reconstructed physically by a reconstruction wave, or completely digitally. Physical reconstructions present many challenges, including complicated lens setups and recording processes [2][pp. 56-60]. Thus digital reconstructions are preferred, since they also enable integration with digital image processing techniques such as machine learning.

Another limitation of traditional imaging systems is that they record only three wavelengths: red, green and blue. This is suitable for human viewing, since the cones in the eye are most sensitive to those wavelengths. However, other spectral information is lost and the spectral resolution is limited. A hyperspectral imaging system (HIS) utilizes several hundreds or thousands of bands. Additional bands are useful in many applications in recognition, including tissue segmentation. Some cells, such as cancerous melanoma cells, absorb a lot of light in the ultraviolet range. Therefore, they can be easily detected even by a handheld scanner. Neittaanmäki et al. demonstrated an 18/19 (94.7%) matching of HIS analysis with histopathological analysis, with 1/19 cases being false positive. Lesion borders were accurately defined in 10/19 (52.6%) of cases.[3]

Hyperspectral holography can be utilized in producing accurate 3D models of cells and microorganisms. Jung et al. presented a method for measuring 3D refractive index tomograms of red blood cells and hepatocytes with a spectral resolution of a few nanometres. [6]. These models can be utilized in molecular biology research.

Since hyperspectral holographic images contain so much information, recognition tasks are best performed with a machine learning algorithm. This is an emerging field of research, and has already provided promising results in segmentation of cancerous cells. Ortega et al. showed proof-of-concept research on applying HIS data to automatically detect brain tumour from pathological slides [4]. They used a spectral range of 400-

1000 nm, extending beyond visible light to infrared. However, a lot of manual work is still required in annotating the training data for the learning algorithm. HIS techniques also augment staining-based cell segmentation well, since absorption is easily distinguishable from a high-resolution spectrum. Zhu et al. constructed a microscope HIS to delineate cancerous gastric cells [5]. They dyed the sample with haematoxylin and eosin (H&E) stain and used the spectral responses to classify the cells. The average accuracy obtained was 95%. The survival rates of cancer patients increase drastically if malignant cells can be detected earlier. In the future hyperspectral holography can be utilized both to augment and to replace human histopathological analysis.

This work describes a method for capturing hyperspectral holographic data with a lensless system and segmenting the data based on spectral analysis. Samples of blood and zebrafish are used to demonstrate the tissue segmentation, along with a phase test target. Advantages of hyperspectral digital holography (HSDH) will be discussed by comparing different segmentation results.

2. THEORY

In wave optics light is treated as waves. Waves can interfere and diffract, and these properties form the basis for holographic acquisition and analysis.

2.1 Wave optics

A simple plane wave propagating in free space can be modelled as [7][p. 3]

$$\psi(x,y,z,t)=Ae^{j(\omega_0 t-\vec{k}_o\cdot\vec{R})}, \tag{1}$$

where $j=\sqrt{-1}$, ω_0 is the angular frequency, $\vec{k}_0$ is the propagation vector and $\vec{R}$ is the position vector. The magnitude of $\vec{k}_0$ is called the wave number. From equation (1), a plane wave propagating in the positive z-direction becomes

$$\psi(z,t)=Ae^{j(\omega_0 t-k_o\cdot z)}. \tag{2}$$

When the plane wave is incident on an aperture, a diffracted field appears. The aperture is represented by a transparency function $t(x,y)$ on the $z=0$ plane. The diffracted field immediately after the aperture is [7][p. 5]

$$\psi(x,y,z=0,t)=At(x,y)e^{j\omega_0 t}=\psi_{p0}(x,y)e^{j\omega_0 t}, \tag{3}$$

where $\psi_{p0}(x,y)$ is called the *complex amplitude*. It is the initial condition used to find the field diffraction away from the aperture, which is written as

$$\psi_p(x,y,z,t)=\psi_{p0}(x,y,z,t)e^{j\omega_0 t}. \tag{4}$$

An example of simple diffraction from a point object is rendered in figure 1.

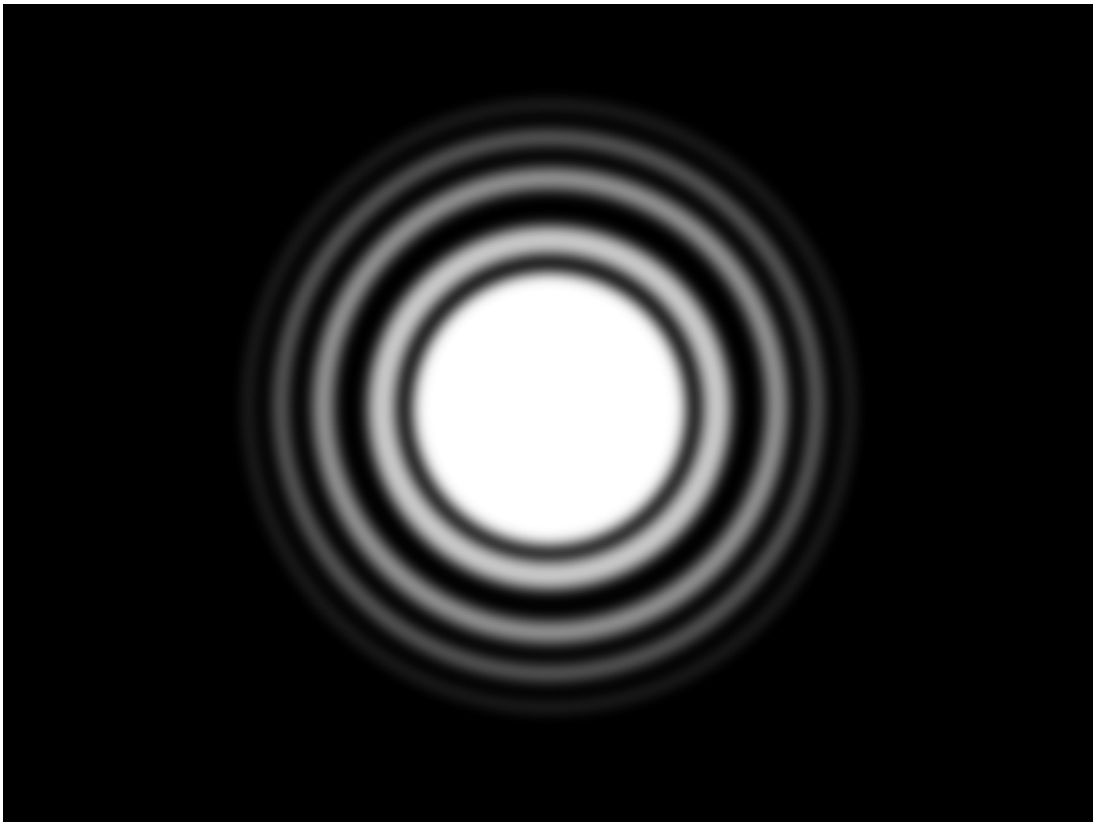

Figure 1: Diffraction from a pinhole aperture.

As the plane waves propagate over a distance ***z***, they acquire a phase shift. The propagated complex amplitude can be solved by Fourier transform [7][p. 9]:

$$\psi_p(x,y;z)=F^{-1}\{\Psi_{p0}(k_x,k_y)e^{-jk_z z}\}=\frac{1}{4\pi^2}\iint_{-\infty}^{\infty}\Psi_{p0}(k_x,k_y)e^{-jk_x x-jk_y y-jk_z z}dk_x dk_y, \tag{5}$$

where F^{-1} is the inverse Fourier transform, $\Psi_{p0}(k_x,k_y)$ is the Fourier transform of $\psi_{p0}(x,y)$ and k_x,k_y are the spatial radian frequency variables. *The spatial frequency transfer function* of propagation is defined as [7][p. 8]

$$H(k_x,k_y;z)=\frac{\Psi_p(k_x,k_y;z)}{\Psi_{p0}(k_x,k_y)}=\exp(-jk_0\sqrt{(1-\frac{k_x^2}{k_0^2}-\frac{k_y^2}{k_0^2})z}), \quad (6)$$

where $\Psi_p(k_x,k_y;z)$ is the Fourier transform of $\psi_p(x,y;z)$.

2.2 Hyperspectral holography

The complex amplitude in equation (3) represents both the amplitude and phase of the light reflected or transmitted by the object. When the light reaches a recording medium, only the intensity of the light is recorded. It is proportional to the complex amplitude squared [7][p. 27]:

$$I=t(x,y)=|\psi_p(x,y)|^2. \quad (7)$$

In a holographic recording, a full complex amplitude is recorded. This is achieved by recording the interference of two waves. One of the waves is diffracted by the object, while the other directly illuminates the recording medium. A spatially coherent light source is required. The recorded intensity is now given by

$$I_H=|\psi_o+\psi_r|^2, \quad (8)$$

where ψ_o is the object wave and ψ_r is the reference wave. When the light source is not monochromatic, the spectral density needs to be also recorded. This is performed by applying Fourier transform spectroscopy, which is discussed more in-depth in [9]. It allows the recording of spectral density along with intensity and phase information, since the supercontinuum laser used contains a range of frequencies.

When the optical path difference between the object and reference waves changes, the interferogram changes accordingly. Mathematically it is expressed as [7][p. 43]

$$I(t)=\langle|A(t)+B(t)|^2\rangle \quad (9)$$

where $\langle\square\rangle$ denotes the time-average integral and $A(r,t)$, $B(r,t)$ are the optical fields. Let $A(t)=A_0(\omega)e^{j\omega t}$ and $B(t)=A_0(\omega)e^{j(\omega t+\tau)}$, a time-delayed version of $A(t)$. According to equation 9,

$$I(t)=\langle|A(t)+B(t)|^2\rangle=2|A_0(\omega)|^2(1+\cos(\omega\tau)). \quad (10)$$

The supercontinuum laser contains a range of frequencies [7][p. 48]

$$E(t)=\int_0^\infty A_0(\omega)e^{j\omega t}d\omega. \tag{11}$$

The temporal Fourier transform of the superposition of $I(t)$ and $E(t)$ yields the equation [7][p. 49]

$$F_\tau\{\Delta I(\tau)\}=P_r(\omega), \tag{12}$$

where $I(\tau)$ is the interferogram with phase shift τ and $P_r(\omega)$ is the spectral density. This result allows the simultaneous recording of complete hyperspectral holographic information. The Fourier transformed recording is a 3D array with spatial frequencies on x- and y-axis, and spectral frequencies on the z-axis.

The intensity of a single point (pixel) shifted from the zero phase shift position can be written as [9]

$$I(x',y',\sigma_m,\delta)=P(\sigma_m)\left|\Psi(x',y',\sigma_m)+e^{-2\pi j\sigma_m\delta}\right|^2, \tag{13}$$

where $I(x',y',\sigma_m,\delta)$ is the point in spectral coordinates x'-y' shifted by δ on the spectral frequency σ_m, $P(\sigma_m)$ is the spectral density and $\Psi(x',y',\sigma_m)$ the complex amplitude. The complete spectrum registered in one point is then

$$G(x',y',\delta)=\Delta\sigma\sum_{m=1}^{M} I(x',y',\sigma_m,\delta), \tag{14}$$

where $\Delta\sigma$ is the spectral interval. By applying Fourier transform to $G(x',y',\delta)$ the complex amplitude on the plane of registration can be written as [9]

$$\Psi(x',y',\sigma_m)=\frac{1}{P(\sigma_m)}\int G(x',y',\delta)e^{(2\pi j\sigma_m\delta)}d\delta. \tag{15}$$

The wavelengths of all planes are resolved from the optical path change between the object and reference waves. In the spectral frequency space the smallest step size is [10][p. 549]:

$$\Delta\sigma_m=\frac{1}{\Delta z\cdot N}, \tag{16}$$

Where Δz is the step size in the holographic recording system and *N* is the total number of recorded planes. The reconstructed wavelengths are then given by [10][p. 549]:

$$\lambda = \frac{1}{\Delta \sigma_m \cdot n_k}, \tag{17}$$

where n_k is the index of the plane in k-space.

2.3 Angular spectrum method

In a lensless system, the diffracted image of the object is reconstructed by back-propagating the recording plane to the object plane. The *angular spectrum method* is used here. It is computationally efficient, requiring only two 2D Fourier transforms. In continuous notation it is written as [7][p. 95]:

$$\psi_p(x, y; z) = F^{-1}\{F\{\psi_{p0}(x, y)\} \cdot H(k_x, k_y; z)\}. \tag{18}$$

Equation (18) can be expressed discretely as [10][p. 549]:

$$P(r\Delta x, s\Delta y) = F^{-1}\left\{F\{P_0(m\Delta x_0, n\Delta y_0)\} e^{\left(-j2\pi d\sqrt{\frac{1}{\lambda^2} - \left(\frac{m}{M\Delta x_0}\right)^2 - \left(\frac{n}{N\Delta y_0}\right)^2}\right)}\right\}, \tag{19}$$

where *P* is the complex reconstruction, Δx and Δy the reconstruction pixel size, *r* and *s* the discrete counting variables in the reconstruction plane, P_0 the complex amplitude in the recording plane, *m* and *n* the discrete counting variables in the recording plane, Δx_0 and Δy_0 the recording pixel size, *d* the propagation distance, λ the wavelength of light and *M* and *N* the pixel numbers.

As an end result, a 3D hyperspectral image cube is obtained. Each x-y plane is an complex amplitude of the object at a single wavelength. Each point in the z-dimension corresponds to a wavelength spectrum and a phase spectrum.

2.4 *k*-means clustering

k-means clustering is a least-squares optimization algorithm for finding the number *k* optimal clusters for a set of vectors [18]. It is commonly implemented iteratively and can be summarized in the following steps:

1. Initialize *k* cluster centres. This is performed either randomly or by an initialization algorithm, such as *k*-means ++ [19]. Using an initialization algorithm results in faster convergence to optimal centres.

2. Compute the euclidean squared distances of all vectors (x_1, x_2, …, x_n) to the centres.

3. Assign each vector to a cluster with the closest centre.

4. Compute the average of all vectors in a cluster to obtain *k* new cluster centres.

5. Repeat steps 2 to 4 until cluster centres do not change or maximum number of iterations is reached.

K-means does not guarantee to find the optimal clusters [20].

3. EXPERIMENT SETUP

The image capturing setup consists of a supercontinuum laser source, beam expander, beam splitters, mirrors, sample holder and a CCD camera. Everything is set up on an anti-vibrational table, because even slight vibrations can corrupt the hyperspectral information. External light sources are turned off to avoid unwanted intensity peaks. Figure 2 shows a diagram of the setup.

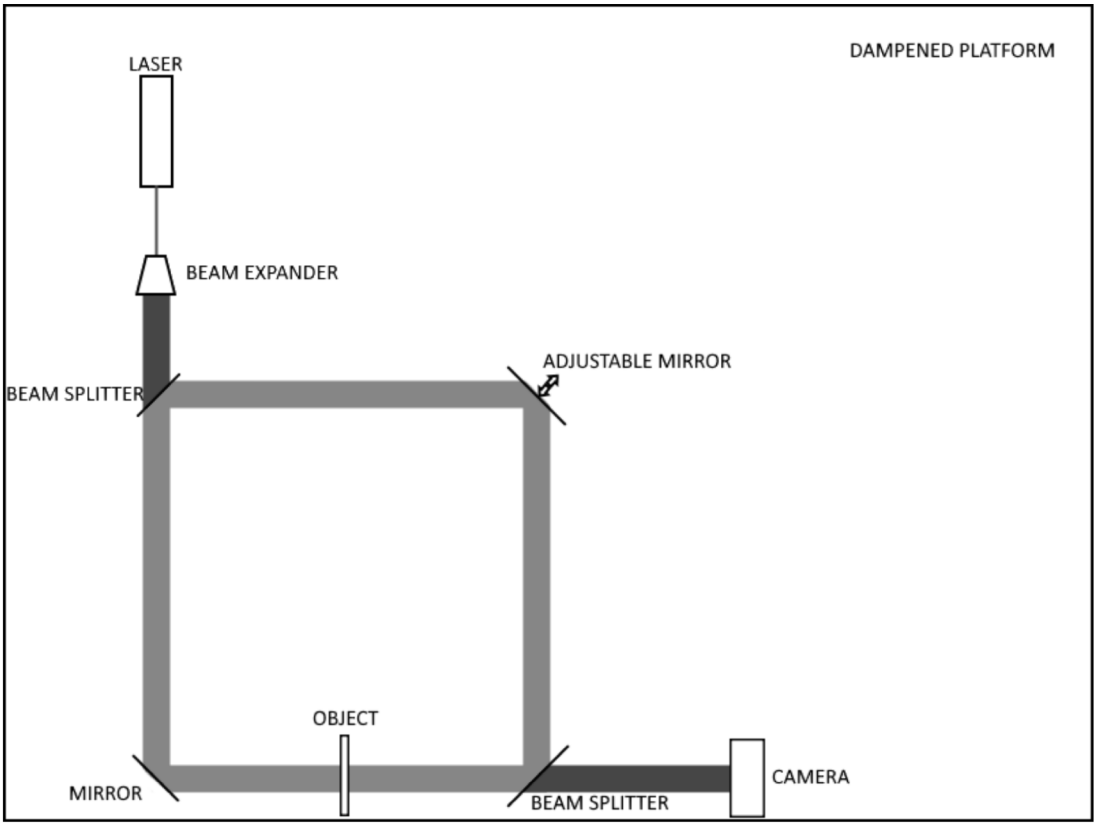

Figure 2: The setup used in the experiment, not to scale.

There are no lenses in the camera. This has the advantage of avoiding chromatic aberration. Using completely digital reconstruction gives more flexibility in the process and allows for easier correction of errors. Reconstruction and segmentation of the images are performed in MATLAB. The phase test object is shown in figure 3.

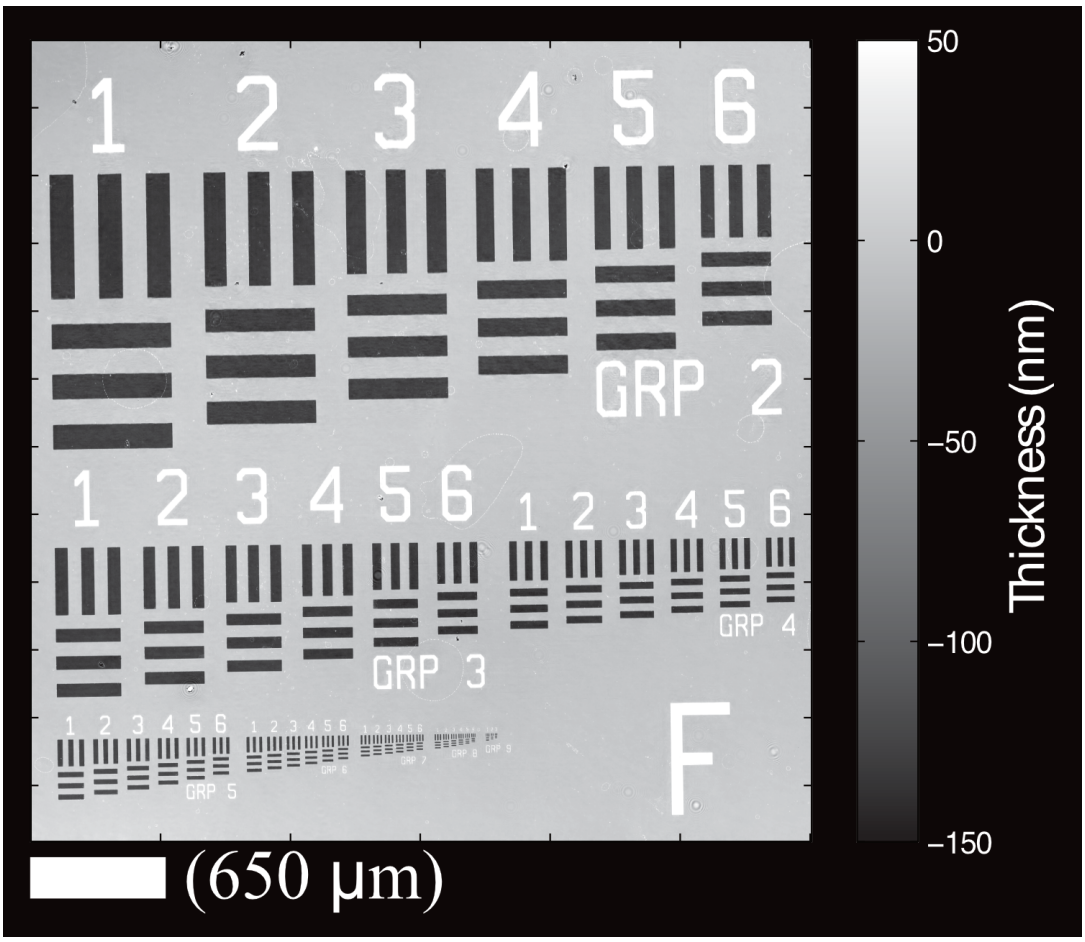

Figure 3: The glass test object used in the experiment [17].

The test object is a clear piece of glass with varying size rectangles etched into it. The rectangles can be clearly seen in a phase image, since their different thickness causes a different phase delay in the light passing through.

3.1 Capturing the diffracted images

One of the mirrors in figure 2 is adjusted by a piezoelectric device. It responds to an increase in voltage by moving away from the zero position. This changes the optical distance between the reference and object arms. The step size of the piezoelectric mirror defines the smallest wavelength that can be resolved, which is two times the step size according to the Nyquist-Shannon sampling theorem [11]. The step size in this experiment is 106.25 nm, and a total of 1128 images are captured, making the total travel distance roughly 120 µm. The piezoelectric stepper used in this experiment exhibited some variation in step size, which was compensated in the reconstruction stage.

The stepper and camera are controlled by a PC and the diffracted images are stored sequentially as the voltage of the piezoelectric device is increased. Images of 4000 by

3000 pixels are captured. The total size of the 1128-image stack is over 18GB, so the images are processed in blocks to conserve system memory.

Before the test samples are captured, the mirror step size is calibrated by using a single-wavelength source and no sample in the holder. The wavelength spectrum of the laser source is acquired by a separate sensor. A stack of images is captured and converted to spectral frequency space as in equation (12). In MATLAB this is performed by calculating the fast Fourier transform (FFT) of each pixel along the z-axis (the depth axis). Because the piezoelectric mirror exhibited a non-linear error in step size across the travel distance, a non-uniform variant of the FFT was used [12]. The correct step size is then calculated by finding the peaks in wavelength- and k-space and using equations (16) and (17). Figure 4 shows the spectra in spatial- and frequency space and highlights the two highest peaks in both. The spectra are reversed with respect to each other because the k-space representation corresponds to the mirror image.

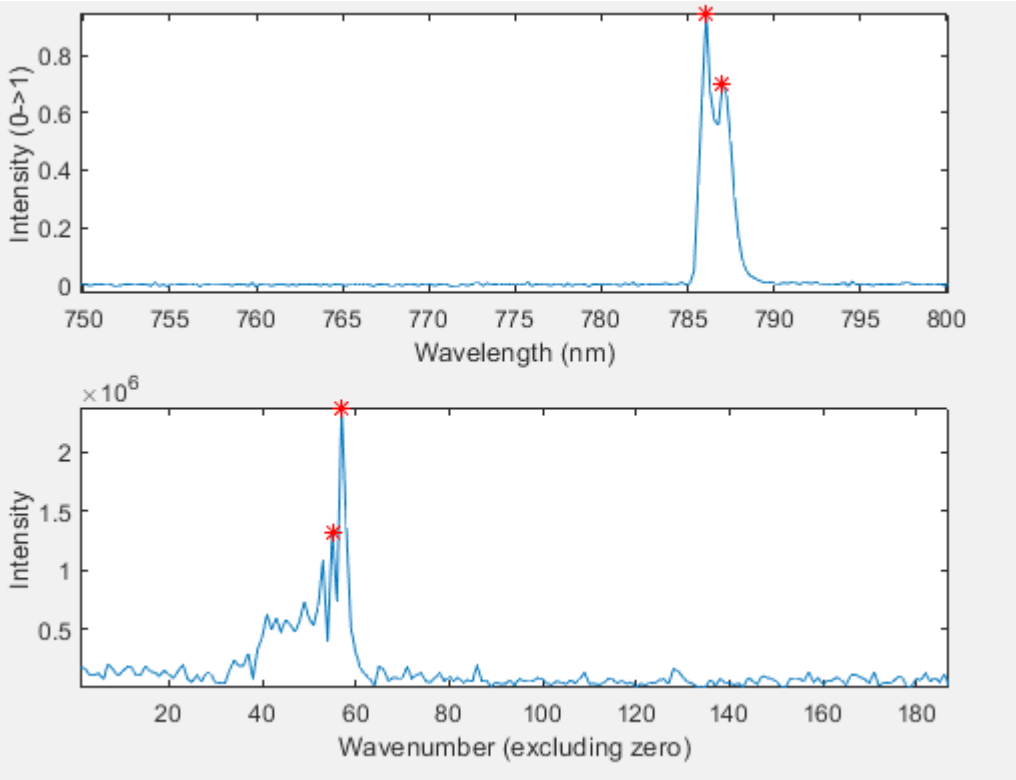

Figure 4: Spatial (top) and spectral (bottom) representation of a sample point in the calibration data.

After the accurate step size value is acquired, the supercontinuum laser source is switched in and a sample in a glass sheet is placed in the sample holder. A stack of images is captured and Fourier transformed along the z-axis, similar to the calibration

data. The wavelength of each plane is calculated using equation (17). Most of the planes do not contain usable information for segmentation, because they are out of the wavelength range of the source (400-1000 nm). They are only needed for better spectral resolution, and are subsequently discarded. Only 70-80 planes have high enough intensity to be used for reconstruction, as shown in figure 5.

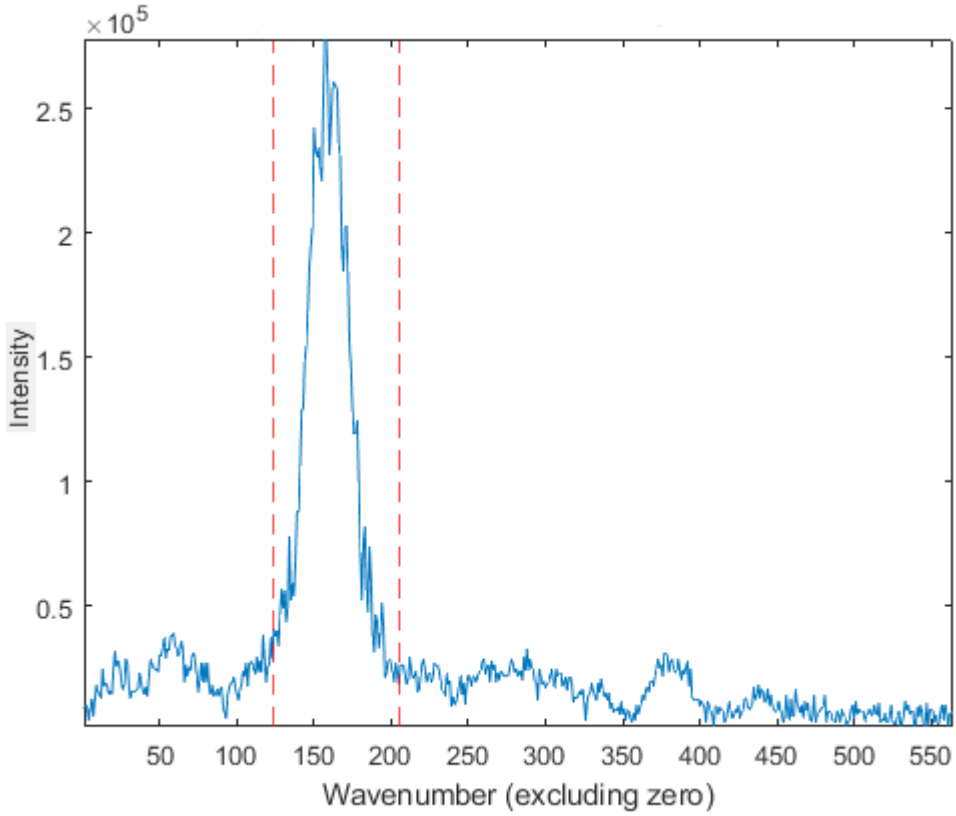

Figure 5: Images selected for reconstruction between the red dotted lines, based on a threshold.

The wavenumbers between the dotted lines in figure 5 correspond to wavelengths of 585nm-986 nm, which is in line with the source and the sensitivity of the camera sensor.

3.2 Preparation and reconstruction

Before reconstruction, some preprocessing is necessary to avoid fringes in the final images. These fringes occur due to aliasing from the high-frequency edges of the plane. The edges need to rolled off with a Gaussian power filter in order to avoid the effect. This process is called *apodization* [14]. Zero padding of about 100 pixels in each dimension is also necessary, depending on the steepness of the filter. The trade-off of

the filtering is that the final images will have reduced intensity on edges, creating a vignette effect. The effects of apodization can be seen in figure 6.

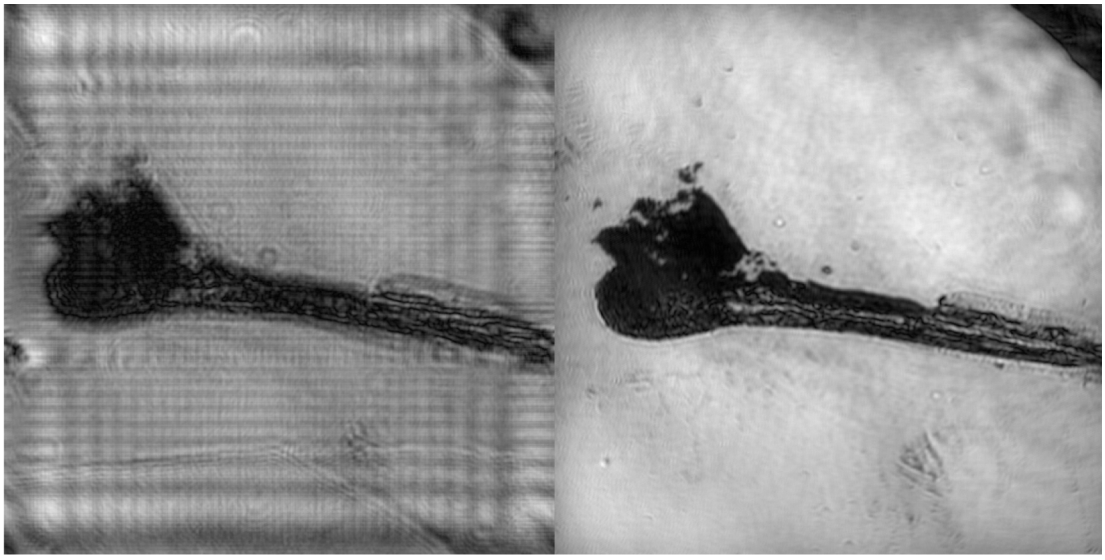

Figure 6: Image without (left) and with (right) apodization.

Next, the correct propagation distance is found by iteration. The distance is different for each sample due to different refracting properties and varying thickness of the glass sheet. It can be found either by manual inspection or by implementing some auto-focus algorithm. In this work a simple method of entropy filtering was implemented to automate the process [13]. First, a plane of sharp intensity is selected and reconstructed using equation (19) with different distances. The resulting image is then filtered with a 9-by-9 entropy filter. The total sum of the filtered image is then compared across different distances. The entropy value becomes high when the image is in focus and low when the image is blurry. Visually, the sharpness can be evaluated by looking at edges and point objects. When the plane is out of focus, circular patterns called *airy disks* [15] appear around point objects as seen in figure 7.

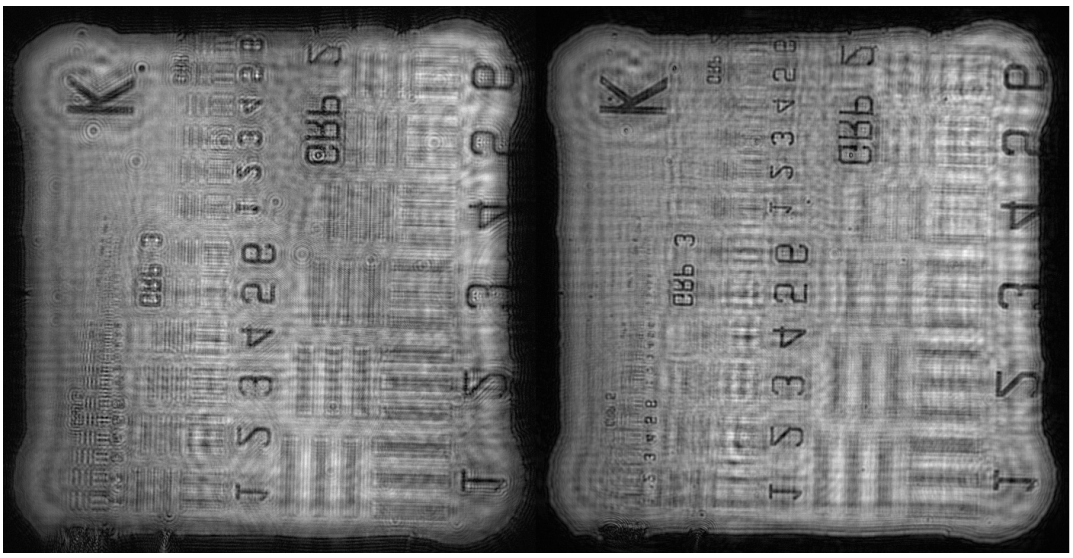

Figure 7: An unfocused image plane (left) where diffraction patterns can be observed and a plane that is in focus (right).

Due to the non-linear step size error described earlier, the wavelengths of each plane are also corrected with the same entropy filtering algorithm. It is necessary that all planes are in focus so that the segmentation is accurate.

Once all the corrected parameters are acquired, the final image stack can be reconstructed by backpropagation as in equation (19). The term inside the square root is set to zero if it is negative to avoid unwanted behaviour at high frequencies. The zero padding introduced in Gaussian filtering is removed after reconstruction.

The final step in reconstruction is correcting a small deviation in inclination in the recording process. Ideally, the light transmitted to the camera would be incident at an exact 90 degree angle. However, in practice there is always a small deviation in the inclination angle. This will cause an uneven phase distribution in the image planes and bias the segmentation results. The deviation is corrected by modelling an inverse inclination and multiplying the plane with it. This will cancel out the inclination. Figure 8 shows the inclination cancellation planes.

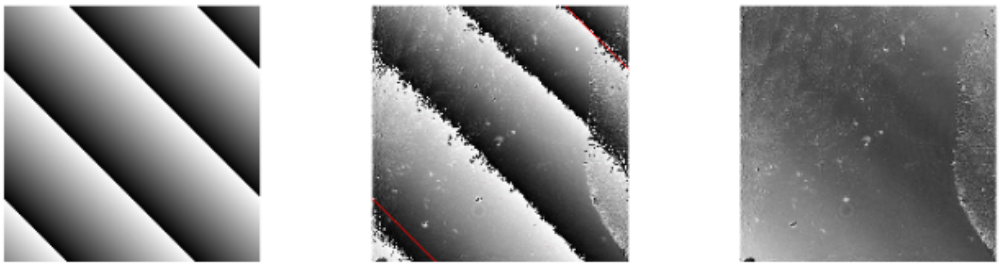

Figure 8: From left to right: artificial plane used to cancel inclination, inclined phase image and the phase image with inclination cancellation.

Some slight fringe patterns can still be seen on the rightmost image, but they are minor enough not to affect the segmentation.

3.3 Segmentation

The reconstructed images are segmented based on both their amplitude and phase. The vignetting caused by apodization is removed by center cropping the image. Adaptive histogram equalization is applied to each plane to reduce the effect of intensity variance between planes. All values are also normalized between 0 and 1. The data is then processed through the MATLAB *kmeans*-algorithm [16], which partitions it into clusters based on mean distances between each point. Each segmentation is done in two parts, first separating only the background from the object(s) and then segmenting the remaining objects.

4. RESULTS

All the samples are captured, processed and segmented as described in chapter 3. The segmentation images are pseudocoloured based on relative differences between clusters, with background being always coloured as black. Segmentations of the glass test target, blood and zebrafish are shown in figures 9, 10 and 11 respectively.

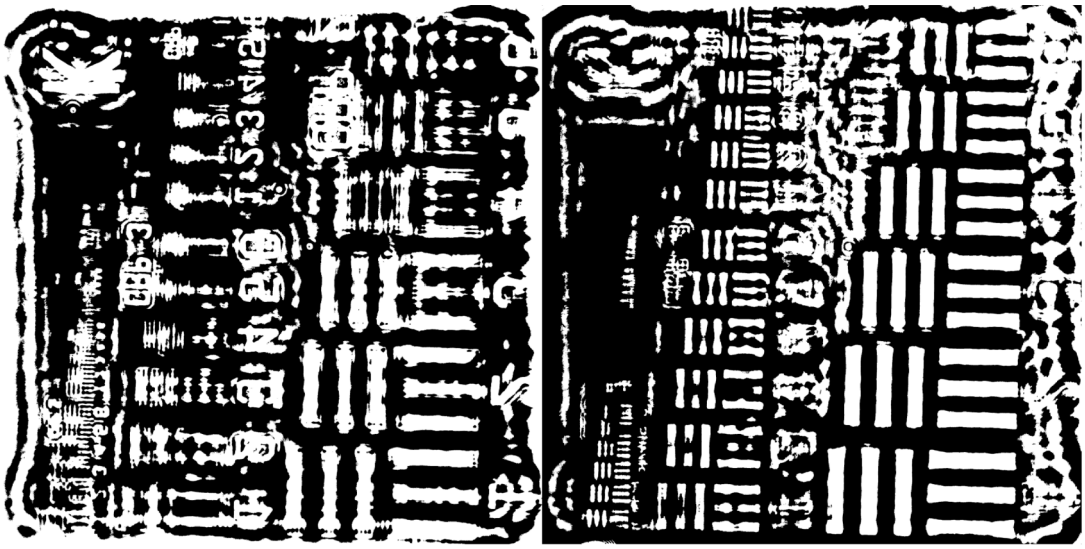

Figure 9: Segmentation of test object with respect to amplitude (left) and phase (right).

In figure 9, it can be seen that the amplitude segmentation highlights the numbers and letters etched on the glass test target, while the phase segmentation is better for showing the engraved lines in the glass. This result demonstrates a clear advantage of using hyperspectral holography for transparent objects.

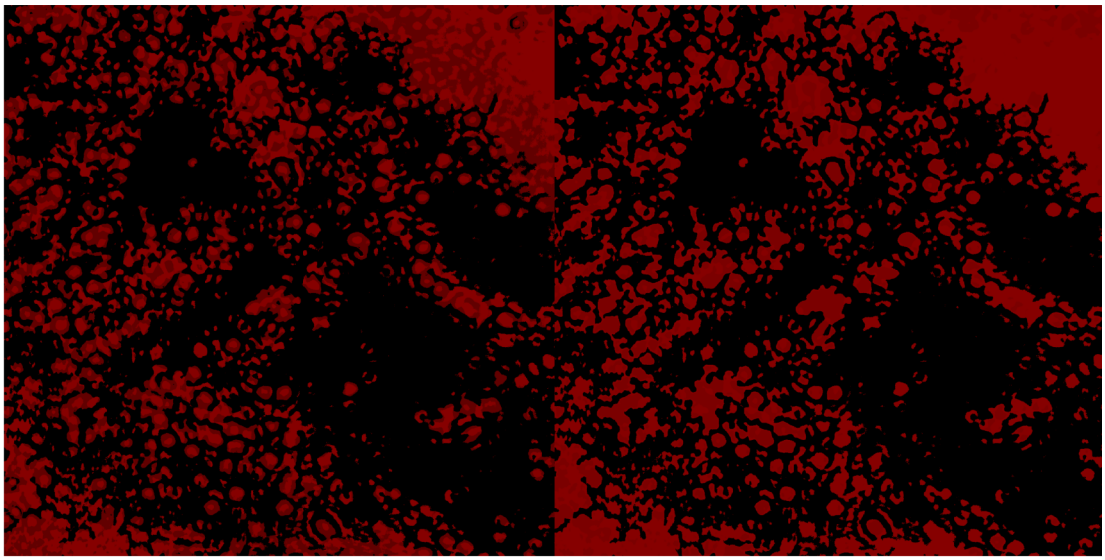

Figure 10: Segmentation of the blood sample with respect to amplitude (left) and phase (right).

The differences in the blood segmentation in figure 10 are more subtle. Individual red blood cells can be seen as bright red circles surrounded by a darker ring. The segmentation consists of mainly red blood cells (individual points) and blood plasma (large connected regions). Platelets are too small to be detected by the camera sensor and white blood cells are so few that they are lost in noise.

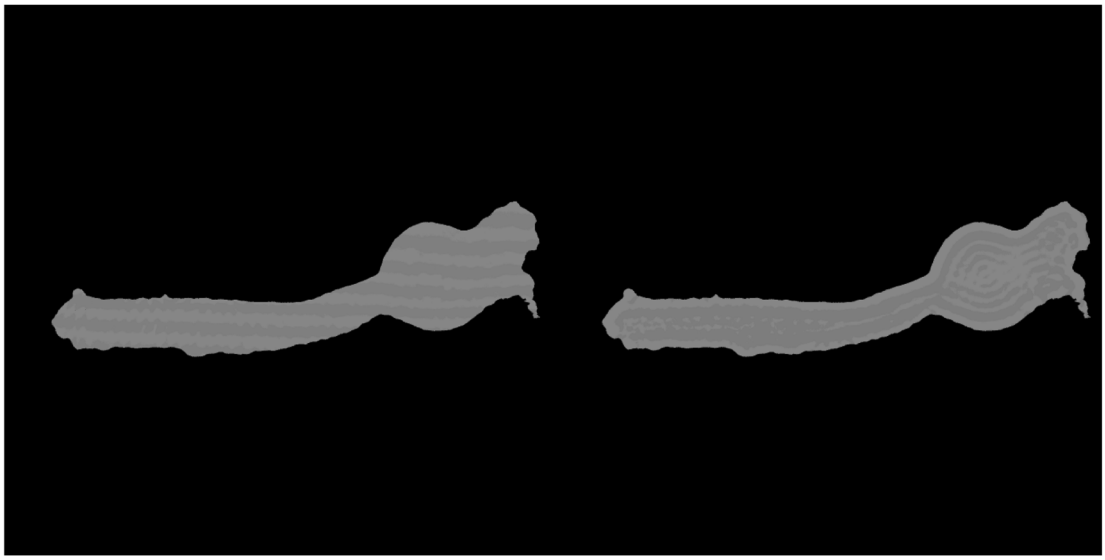

Figure 11: Segmentation of the zebrafish sample with respect to amplitude (left) and phase (right).

The zebrafish segmentation in figure 11 shows nothing of much interest aside from the fish being separated from the background. The experiment setup in this work is not able to capture thick objects, such as the zebrafish sample, very well. Higher resolution or a more powerful light source would be needed to capture the zebrafish.

5. CONCLUSION

Hyperspectral digital holography is a promising tool for tissue segmentation and other applications in biotechnology. The results show that the inclusion of the complete complex amplitude and a wide wavelength spectra allows for more accurate segmentation than is possible with traditional methods. The advantages are apparent especially in transparent objects, such as the glass test target and blood sample. In this work the k-emans clustering was able to provide good results even with single samples. HSDH could also be potent in label free applications, where staining chemicals cannot be used. A potential problem could be the sensitivity of the recording process to external disturbances. In laboratory conditions this is not an issue, but it needs to be taken into consideration in practical applications.

The use of machine- or deep learning algorithms was out of the scope of this work. They are also a considerable addition to the process, especially when many tissue samples are available.

REFERENCES

[1] D. Gabor. 'A New Microscopic Principle', Nature, 161: 777–778, 1948. Available at: https://www.nature.com/articles/161777a0 (Referenced 1.10.2019)

[2] T. Poon. 'Optical Scanning Holography With MATLAB', Springer, 2007.

[3] N. Neittaanmaki-Perttu, M. Grönroos, L. Jeskanen, I. Pölönen, A. Ranki, O. Saksela & E. Snellman. 'Delineating Margins of Lentigo Maligna Using a Hyperspectral Imaging System', Acta Derm Venereol, 95: 549–552, 2015.

[4] S. Ortega, H. Fabelo, R. Camacho , M. De La Luz Plaza , G. M. Callico & R. Sarmiento. 'Detecting brain tumor in pathological slides using hyperspectral imaging', Biomedical Optics Express , 818: Vol. 9 No. 2, 2018.

[5] S. Zhu, K. Su, Y. Liu, H. Yin, Z. Li, F. Huang, Z. Chen, W. Chen, G. Zhang & Y. Chen. 'Identification of cancerous gastric cells based on common features extracted from hyperspectral microscopic images', Biomedical Optics Express, 1135: Vol. 6 No. 4, 2015.

[6] J. Jung, K. Kim, J. Yoon & Y. Park. 'Hyperspectral optical diffraction tomography', Optics Express, 2006: Vol. 24 No. 3, 2016.

[7] T. Poon & J. Liu. 'Introduction to Modern Digital Holography with MATLAB', Cambridge University Press, 2014.

[8] T. Poon & P. P. Banerjee. 'Contemporary Optical Image Processing with MATLAB', Elsevier, 2001.

[9] S. G. Kalenkov, G. S. Kalenkov & A. E. Shtanko. 'Hyperspectral holography: an alternative application of the Fourier transform spectrometer', Journal of the Optical Society of America, Vol. 34 No. 5, 2017.

[10] D. Claus, G. Pedrini, D. Buchta & W. Osten. 'Accuracy enhanced and synthetic wavelength adjustable optical metrology via spectrally resolved digital holography', Journal of the Optical Society of America, Vol. 35 No. 4, 2018.

[11] C.E. Shannon. 'Communication in the Presence of Noise', Proceedings of the Institute of Radio Engineers, Vol. 37. Available at https://ieeexplore.ieee.org/document/1697831 (Referenced 11.11.2019)

[12] M. Ferrara. 'NUFFT, NFFT, USFFT', Mathworks File Exchange, 2009 (Referenced on 12.11.2019), based on L. Greengard & J. Lee, 'Accelerating the Nonuniform Fast Fourier Transform', SIAM Review, Vol. 46 No. 3, 2004.

[13] MATLAB Documentation. 'entropyfilt, Local entropy of grayscale image'. Available at https://www.mathworks.com/help/images/ref/entropyfilt.html (Referenced 12.11.2019)

[14] F.J. Harris. ‘On the use of windows for harmonic analysis with the discrete Fourier transform’, Proceedings of the IEEE, Vol. 66 No. 1, 1978.

[15] G. B. Airy. ‘On the Diffraction of an Object-glass with Circular Aperture’, Transactions of the Cambridge Philosophical Society, Vol. 5 pp. 283-291, 1835.

[16] MATLAB Documentation. ‘kmeans, k-means clustering’. Available at https://www.mathworks.com/help/stats/kmeans.html (Referenced 19.11.2019)

[17] T. M. Godden, A. Muñiz-Piniella, James Claverley, Andrew Yacoot, and M. J. Humphry. ‘A phase calibration target for quantitative phase imaging with ptychography’, Optics Express (submitted) 2016.

[18] S.P. Lloyd. ‘Least Squares Quantization in PCM ‘, IEEE Transactions on Information Theory, Vol. 28 pp. 129-137, 1982.

[19] A. David & S. Vassilvitskii. ‘K-means++: The Advantages of Careful Seeding‘, SODA ‘07: Proceedings of the Eighteenth Annual ACM-SIAM Symposium on Discrete Algorithms, pp. 1027-1035, 2007.

[20] J.A. Hartigan, M.A Wong. ‘Algorithm AS 136: A k-Means Clustering Algorithm’, Journal of the Royal Statistical Society, Series C, Vol. 28 pp. 100-108, 1979.